Symmetry Breaking in Time-Dependent Billiards

Anne Kétri Pasquinelli da Fonseca*, Edson Denis Leonel
Departamento de Física, Universidade Estadual Paulista (UNESP), Avenida 24A, 1515, Bela Vista, Rio Claro, 13506-900, São Paulo, Brazil.

* Corresponding author. Email: anne.ketri@unesp.br (A.K.P.F.); edson-denis.leonel@unesp.br (E.D.L.)
Manuscript submitted May 20, 2025; accepted June 23, 2025; published August 15, 2025.
doi: 10.17706/ijapm.2025.15.2.78-90

Abstract: We investigate symmetry breaking in a time-dependent billiard that undergoes a continuous phase transition when dissipation is introduced. We provide the identification of symmetry breaking explicitly linked to the boundary velocity limits in time-dependent billiards, resolving the open question of fully characterizing this phase transition. The system presents unlimited velocity, and thus energy growth for the conservative dynamics. When inelastic collisions are introduced between the particle and the boundary, the velocity reaches a plateau after the crossover iteration. The system presents the expected behavior for this type of transition, including scale invariance, critical exponents related by scaling laws, and an order parameter approaching zero in the crossover iteration. We analyze the velocity spectrum and its averages for dissipative and conservative dynamics. The transition point in velocity behavior caused by the physical limit of the boundary velocity and by the introduced dissipation coincides with the crossover interaction obtained from the root-mean squared velocity, or V_{rms}, curves. Additionally, we examine the velocity distributions, which lose their symmetry once the particle's velocity approaches the lower limit imposed by the boundary's motion and the system's control parameters. This distribution is also characterized analytically by an expression $P(V, n)$, which attains a stationary state, with a well-defined upper bound, only in the dissipative case.

Keywords: Time-dependent billiards, symmetry breaking, phase transitions, dynamical systems

1. Introduction

Phase transitions have been extensively studied for more than a century, with applications spanning various physical systems. From the development of thermodynamics in the 19th century to the statistical mechanics of the 20th century, the concept of phase transitions has evolved to encompass increasingly complex phenomena [1]. A significant milestone was the identification of phase transitions that involve the breaking of continuous symmetries, most notably the Bose-Einstein condensation observed in ideal Bose gases as the temperature is lowered at a fixed positive density, and subsequently focus on systems with discrete symmetries, such as the Ising model [2]. Currently this concept has found several relevant applications in quantum many-body physics [3, 4], ultra-cold atomic systems [5], high-energy physics [6], information theory [7, 8] and, as in this case, dynamical systems [9–11].

Different phases of a system can usually be assigned to different symmetries: the sudden rearrangement of a crystal lattice changes the state of the body discontinuously between different phases [12]. These changes in symmetry may also happen continuously, in second-order, also called continuous phase transitions, named after the corresponding order of the free energy derivative that breaks continuity during the transition [13].

We can refer quantitatively to this change in symmetry, defining the quantity called "order parameter", which continuously approaches zero as the system reaches the transition point [12].

These continuous phase transitions are also characterized by their scale invariance, with critical exponents related by scaling laws, and which do not depend on the microscopic details of the system, but only on its dimensionality and symmetry, a phenomenon known as universality [14]. Such examples of these transitions are the Ising model, where the magnetization vanishes as the temperature is raised until it's critical value [11], and the transition from integrability to non-integrability for the standard dissipative mapping [15], where it changes from regular to chaotic behavior in the phase space.

As mentioned, a key step to characterize such phase transitions is to identify the symmetry broken at the critical point, which marks a qualitative change in the system's macroscopic behavior [11]. While symmetry breaking has been studied in two-dimensional systems, such as the dissipative standard map, where it arises from the destruction of invariant curves near the transition from integrability to chaos [16], limited attention has been paid to its role in mixed-phase-space billiards [17, 18]. In such billiards, the phase transition from conservative to dissipative dynamics remains to be understood, particularly how symmetry breaking emerges from the introduction of time dependency on the boundary and inelastic collisions. In this work, we characterize such symmetry breaking explicitly, detailing the mechanisms responsible for leading the system from the conservative to the dissipative case.

A billiard is a dynamical system composed of a particle or a set of non-interacting particles suffering specular collisions with a rigid boundary that confines them [19]. The shape of the boundary plays a fundamental role in determining the system's behavior. Depending on its geometry, the dynamics can range from fully integrable, as in the case of the circular billiard [20, 21], to fully chaotic, as exemplified by the Sinai billiard and the Bunimovich stadium [22, 23], or exhibit a mixed phase space structure, as seen in the oval billiard [24]. Billiards can be framed by Hamiltonians such as $H(x,p,t)=\frac{p^2}{2m}+V(x,t)$, where $V(x,t)=V_0(x)+V_1(x,t)$. The component $V_1(x,t)$ is associated with the time-dependency introduced in the boundary, leading to non-integrability [25].

Although seemingly very simple, these systems offer a wide array of potential applications across diverse fields, including optics and photonics [17, 26], plasma physics [18], electronic transport [27], complex networks [28], and condensed matter physics [29]. Therefore, characterizing its symmetry breaking is extremely important for better understanding the mechanisms behind these systems' phase transitions.

In this work, we investigate the symmetry breaking in an oval-shaped billiard as it goes from unbounded to bounded diffusion as dissipation is introduced. The boundary is given by $R_b(\theta,t)=1+\epsilon[1+\eta\cos(t)]\cos(p\theta)$, where ϵ controls the integrability of the system and η gives the amplitude of the temporal dependence. A discrete four-dimensional mapping T describes the systems dynamics. The system is integrable system for ϵ=0 and presents mixed dynamics for $\epsilon \neq 0$ [19]. The Loskutov-Ryabov-Akinshin (LRA) conjecture determines that the existence of chaos in the phase space is a sufficient, not necessary, condition for the occurrence of an unlimited energy growth when a time perturbation of the boundary is introduced [30, 31]. This energy growth is also known as Fermi Acceleration (FA). This phenomenon can be suppressed by introducing dissipation, in this case in the form of inelasticity in the collisions characterized by a restitution coefficient γ.

In the conservative case, the particle velocities exhibit FA due to diffusive behavior, while the dissipative case leads the system to a stationary state. We show that the onset of this transition is governed by the boundary velocity's physical limit and the dissipation's strength, as revealed by the V_{rms} and $\overline{V}$ curves. The velocity distribution becomes asymmetric near its lower bound, determined by the system's control parameters, and reaches a stationary profile only in the dissipative regime. This behavior is also recovered by the analytical distribution $P(V,n)$ near this transition.

This paper is organized as follows: Section 2 describes the model for the time-dependent oval billiard and discusses its velocities behavior, along with scaling properties. Sections 3 and 4 present the behavior of such velocities for the conservative and dissipative case, respectively, as well as the velocities distributions for each instances, comparing with the established results for this system. Section 5 presents the final discussions and conclusions regarding the symmetry breaking.

2. The Model and the Mapping

As mentioned, the main focus of this work is the oval billiard. The boundary is given, in polar coordinates, by $R_b(\theta, t) = 1 + \epsilon[1+\eta\cos(t)]\cos(p\theta)$, where θ is the polar angle, ϵ is a parameter controlling the circle deformation, η gives the amplitude of the time perturbation, and p deforms the boundary. We limit our analysis to integer values of p, as non-integer values would lead to the existence of holes in the boundary, allowing the escape of particles and going beyond the scope of this work. $\epsilon = 0$ retrieves the circular billiard, which we know to be fully integrable, while $\epsilon \neq 0$ leads to a mixed phase space, containing both chaos, periodic islands, and invariant spanning curves [24]. The further increase of ϵ leads to the vanishing of these regular structures, being fully chaotic for values above $\epsilon_c = \frac{1}{1+p^2}$ [32]. The time-dependent boundary $\eta \neq 0$, as defined by the LRA conjecture [31], leads to unbounded diffusion caused by chaotic dynamics for the static regime.

We can write a four-dimensional nonlinear mapping $T(\theta_n, \alpha_n, V_n, t_n)$ welding the dynamics of the impact n with $n + 1$. θ, as mentioned, represents the polar angle relative to the origin of the coordinate system, while α corresponds to the angle between the trajectory and the vector tangent to the boundary. V and t represent, respectively, the velocity of the particle and the instant of impact. The coordinates for the particle are given by $X(\theta_n) = R(\theta_n, t_n)\cos(\theta_n)$ and $Y(\theta_n) = R(\theta_n, t_n)\sin(\theta_n)$. The velocity is then written as:

$$\overrightarrow{V_n} = \left|\overrightarrow{V_n}\right|[\cos(\phi_n + \alpha_n)\,\hat{\imath} + \sin(\phi_n + \alpha_n)\,\hat{\jmath}], \tag{1}$$

where ϕ_n=arctan $[Y'(\theta_n, t_n)/X'(\theta_n, t_n)]$ is an auxiliary angle, with primes denoting partial derivatives over θ_n. The specular reflection law must also be obeyed, for the non-inertial referential frame of the moving boundary, this is written as:

$$\vec{V}'_{n+1} \cdot \vec{T}_{n+1} = \vec{V}'_n \cdot \vec{T}_{n+1} \tag{2}$$

$$\vec{V}'_{n+1} \cdot \vec{N}_{n+1} = \vec{V}'_n \cdot \vec{N}_{n+1} \tag{3}$$

where $\vec{T}$ and $\vec{N}$ indicate the unit vectors for the tangential and normal components, respectively, written as $\vec{T}_{n+1} = cos(\phi_{n+1})\hat{\imath} + sin(\phi_{n+1})\hat{\jmath}$ and $\vec{N}_{n+1} = -sin(\phi_{n+1})\hat{\imath} + cos(\phi_{n+1})\hat{\jmath}$. With these equations, the velocity at the $(n + 1)^{th}$ collision is finally written as:

$$\left|\vec{V}_{n+1}\right| = \sqrt{\left(\vec{V}_{n+1} \cdot \vec{T}_{n+1}\right)^2 + \left(\vec{V}_{n+1} \cdot \vec{N}_{n+1}\right)^2}. \tag{4}$$

The trajectory of the particle is given by:

$$X(t) = X(\theta_n, t_n) + \left|\vec{V}_n\right| \cos(\alpha_n + \phi_n)\,(t - t_n), \tag{5}$$

$$Y(t) = Y(\theta_n, t_n) + \left|\vec{V}_n\right| \sin(\alpha_n + \phi_n)\,(t - t_n). \tag{6}$$

Fig. 1 shows, for the static case, different boundary shapes for different parameters ϵ and p, as well as for the trajectory of a single particle in item (c) and the normal and tangential components in item (d).

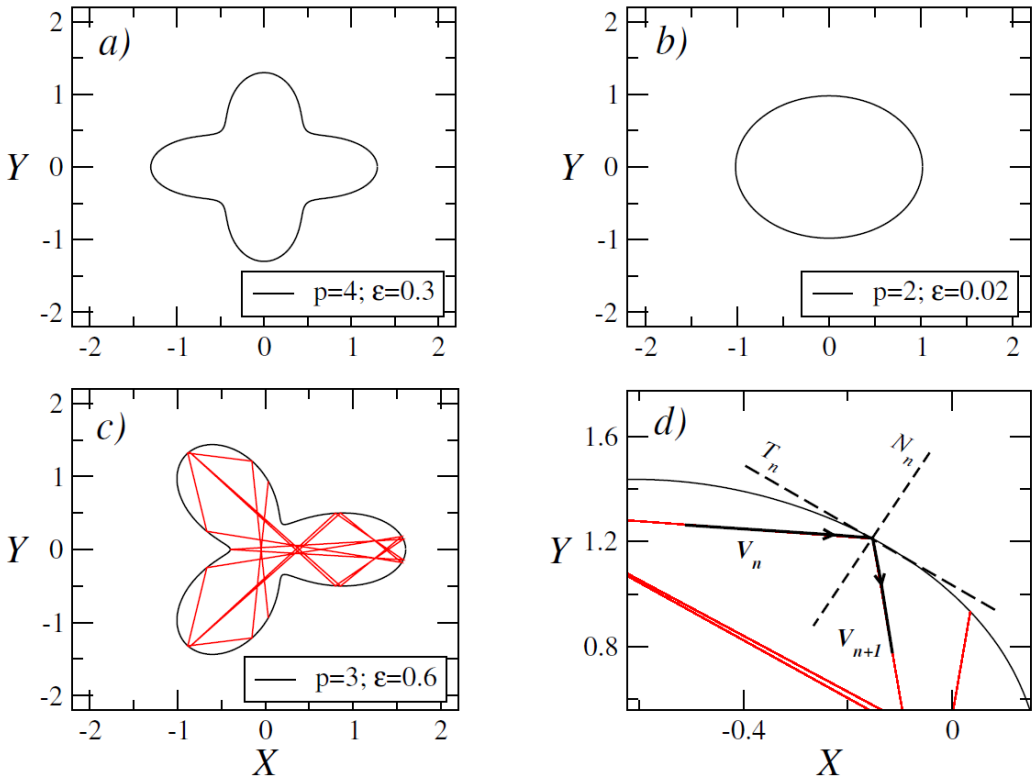

Fig. 1. (Color online) Different boundary shapes, trajectories, velocities, normal and tangential components for different parameters ϵ and p. Figs. 1a)–d) show boundary shapes for different combinations of parameters ϵ and p. c) and d) also show the trajectory for a single particle, in red. The normal and tangential components, as well as the velocities V_n and V_{n+1} are also presented in d).

The position of the particle can then be obtained by $R(t) = \sqrt{X^2(t) + Y^2(t)}$. The point of collision is found when $R = R_b$. After the collision, the updated angle α_{n+1} is given by $\alpha_{n+1} = \arctan[\vec{V}_{n+1} \cdot \vec{N}_{n+1} / \vec{V}_{n+1} \cdot \vec{T}_{n+1}]$. As for the velocity of the moving boundary, it can be written as [33]:

$$|\vec{V}_b(t_{n+1})| = \frac{dR(t)}{dt}|_{t_{n+1}}[cos(\theta_{n+1})\hat{\imath} + sen(\theta_{n+1})\hat{\jmath}] \propto \epsilon\eta \tag{7}$$

To analyze the particle velocities V_n, it is convenient to recur to two new quantities: $\overline{V}$ and V_{rms}. For M different initial conditions and n collisions of the particle with the boundary, they are written as:

$$V_{rms} = \sqrt{\overline{V^2}(n)} = \sqrt{\frac{1}{M}\sum_{i=1}^{M}\frac{1}{n}\sum_{j=1}^{n}V_{i,j}^2} \tag{8}$$

Here $V_{i,j}$ represents the velocities for each trajectory i and for all j different orbits.

For the conservative case, as shown in Fig. 2a), the behavior of V_{rms} can be summarized as follows: (i) $V_{rms} \propto n^{\beta}$ with $\beta \approx 0.5$ for small values of V_0; (ii) A plateau $\overline{V}_{plat} \propto V_0^{\zeta}$ is observed for $n \ll n_x$, where $\zeta \approx 1$; (iii) the crossover iteration between (i) and (ii) is given by $n_x \propto V_0^z$, with $z \approx 2$. The scale invariance observed

in the system allows us to, using a homogeneous and generalized function $\langle\overline{V}\rangle(n, V_0) = l\langle\overline{V}\rangle(l^a n,\ l^b V_0)$, write a scaling law relating the three exponents $z = \zeta/\beta$. These exponents, as is the case for similar systems, are universal and not geometry dependent [34]. The overlap of the curves into a single universal one can be done using the scaling transformations $V_{rms} \rightarrow V_{rms}/V_0^{\zeta}$ and $n \rightarrow n/V_0^{z}$. The universal plot is given in Fig. 2b). As mentioned, the conservative case leads to unlimited velocity and, thus, energy growth, known as FA. Our chosen method to suppress this behavior is to consider the collisions of the particles with the boundary to be inelastic. The dissipation is introduced by a restitution coefficient $\gamma < 1$ in the normal component of the velocity. For $\gamma = 1$, the collisions are elastic, returning to the conservative case. The updated reflection law is:

$$\vec{V}_{n+1} \cdot \vec{N}_{n+1} = -\gamma \vec{V}_n \cdot \vec{N}_{n+1} + (1+\gamma)\vec{V}_b[t_{n+1} + Z(n)] \cdot \vec{N}_{n+1} \tag{9}$$

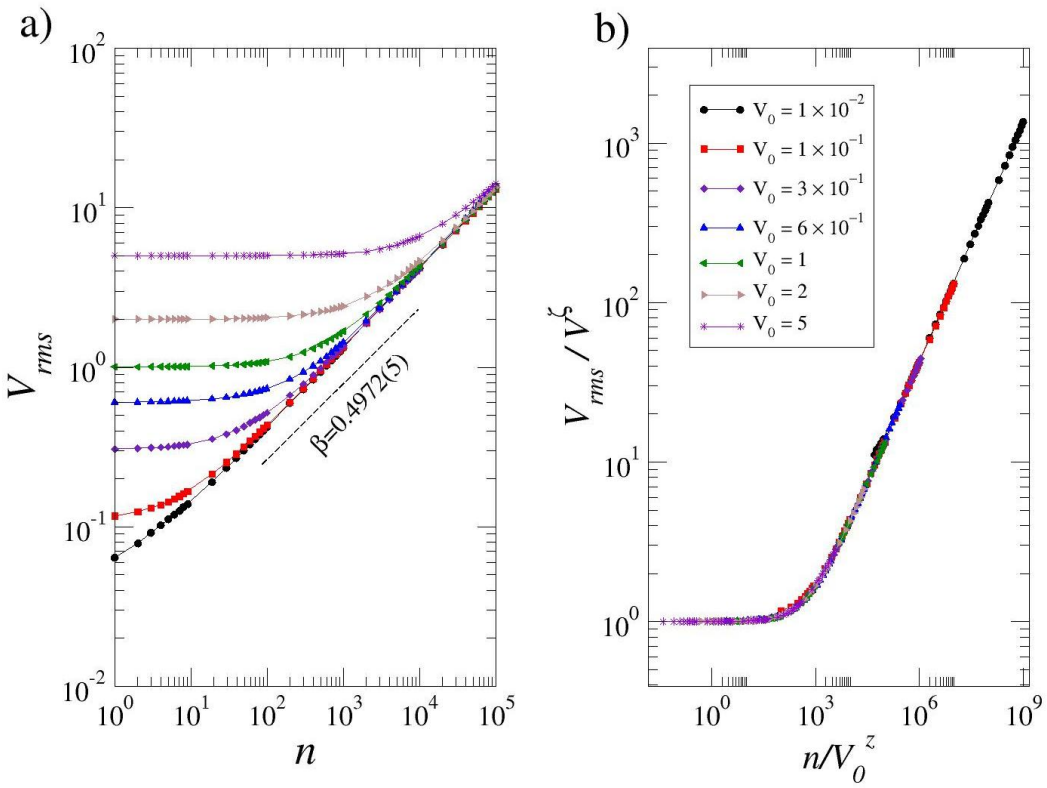

Fig. 2. (Color online)V_{rms} curves for a set of different initial velocities V_0 and their subsequent overlap using the scaling transformations (conservative case). (a) V_{rms} vs. n constructed from the mapping for and $\epsilon = 0.08$, $p = 3$, $\eta = 0.5$ and different values of V_0. (b) Overlap of the curves in (a) into a single universal curve using the scaling transformations $V_{rms} \rightarrow V_{rms}/V_0^{\zeta}$ and $n \rightarrow n/V_0^{z}$.

Fig. 3a) shows that fractional energy loss does indeed suppress the FA. We can now write a new set scaling hypotheses as: (i) $V_{rms} \propto [(\eta\epsilon)^2 n]^{\beta}$ or $n \ll n_x$, with $\beta \approx 0.5$; (ii) the velocity reaches a plateau described by $\overline{V}_{sat} \propto (1-\gamma)^{\zeta_1}(\eta\epsilon)^{\zeta_2}$, for $n \gg n_x$, where $\zeta_1 \approx -0.5$ and $\zeta_2 \approx 1$; (iii) the crossover iteration is given by $n_x \propto (1-\gamma)^{z_1}(\eta\epsilon)^{z_2}$, with $z_1 \approx -1$ and $z_2 \approx 0$. The two scaling laws for this case are $z_1 = \frac{\zeta_1}{\beta}$ and $z_2 = \frac{\zeta_2}{\beta} - 2$. Again the overlap of the curves into a single universal one can be done using scaling transformations: $V_{rms} \rightarrow V_{rms}/(1-\gamma)^{\zeta_1}(\eta\epsilon)^{\zeta_2}$ and $n \rightarrow n/(1-\gamma)^{z_1}(\eta\epsilon)^{z_2}$. The curves overlap into a single universal plot, is given in Fig. 3b).

It's worth mentioning that, in both the conservative and dissipative case, the exponent $\beta \approx 0.5$ indicates diffusive growth in velocity, typical of stochastic energy transfer in chaotic systems. This behavior is consistent with the universality class of Fermi acceleration in time dependent billiards and reflects weak anomalous diffusion in velocity space prior to saturation [33]. The fact that the same exponent appears in both regimes suggests that the dynamics in $n \ll n_x$ is governed by the same fundamental mechanism of chaotic energy transfer from the boundary to the particle.

Our main goal in this analysis is to investigate the broken symmetry between the two regimes, examining how the velocity distributions, and their associated averages, relate to V_{rms}, as will be discussed in the following sections.

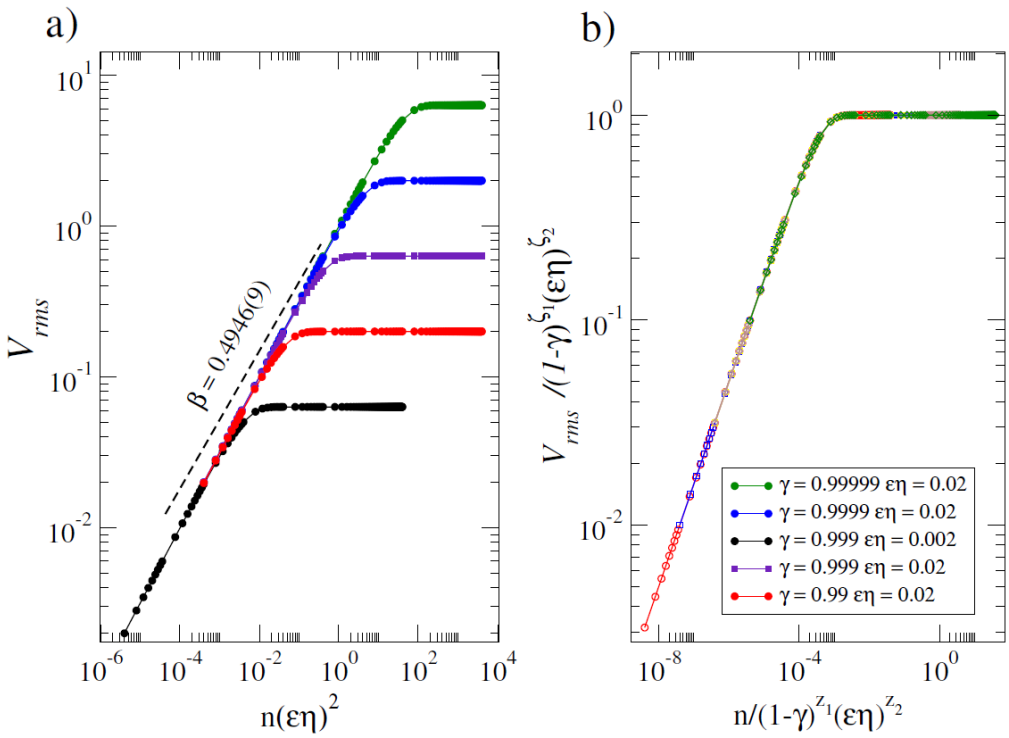

Fig. 3. (Color online) curves for a set of different control parameters γ and $\epsilon\eta$, with their subsequent overlap obtained through the scaling transformations (dissipative case). (a) V_{rms} vs. $n(\epsilon\eta)^2$ constructed from the mapping for initial velocity $V_0 = 10^{-5}$ for different values of γ and $\eta\epsilon$. (b) Overlap of the curves in (a) into a single universal curve using the scaling transformations $V_{rms} \to V_{rms}/(1-\gamma)^{\zeta_1}(\eta\epsilon)^{\zeta_2}$ and $n \to n/(1-\gamma)^{z_1}(\eta\epsilon)^{z_2}$.

3. Conservative Case

We begin this characterization exploring the underlying symmetry properties of the system in the absence of dissipation. We aim to answer how the velocity distribution behaves in this regime, and what it can reveal about the mechanisms responsible for symmetry breaking.

We examine both the root-mean-square velocity (V_{rms}) and the complete velocity distribution. Fig. 4 shows, for the first 100 collisions, the trajectories of 10 different initial conditions (θ_n, α_n) randomly chosen from $[0, 2\pi]$ for $V_0 = 1$, $\epsilon = 0.08$, $\eta = 0.5$ and $\gamma = 1$. The curves were constructed from a direct solution of the mapping equations described in Section 2, with collision instants and positions determined via the bisection method, using a tolerance on the order of 10^{-12}. The maximum and minimum values reached from these trajectories are saved, leading to the purple and turquoise lines, named V_{max} and V_{min}, respectively. The V_{rms} curve is green, still in the plateau region, as observed in Fig. 2. The average values of the velocity for the regions above

and below V_{rms} are shown in the blue and red curves, respectively. We refer to these quantities as $\overline{V}_{max}$ and $\overline{V}_{min}$.

In agreement with the plateau observed for V_{rms}, the distribution of velocities of each trajectory is distributed symmetrically around the initial value V_0. The curves of V_{max}, V_{min}, $\overline{V}_{max}$ and. $\overline{V}_{min}$ also present such symmetry. Fig. 5 presents the evolution of the five curves V_{rms}, V_{max}, V_{min}, $\overline{V}_{max}$ and $\overline{V}_{min}$ for $V_0 = 0.6$, $\epsilon = 0.08$, $\eta = 0.5$, $p = 3$, $\gamma = 1$ and $n = 10^4$ collisions. The symmetric behavior between the curves $\overline{V}_{max}$ and $\overline{V}_{min}$ is broken after approximately 200 collisions, as highlighted in panel b). As observed in Fig. 6 increasing the value of n leads to a gradual flattening of the curve, eventually reaching a lower limit for the particle velocities.

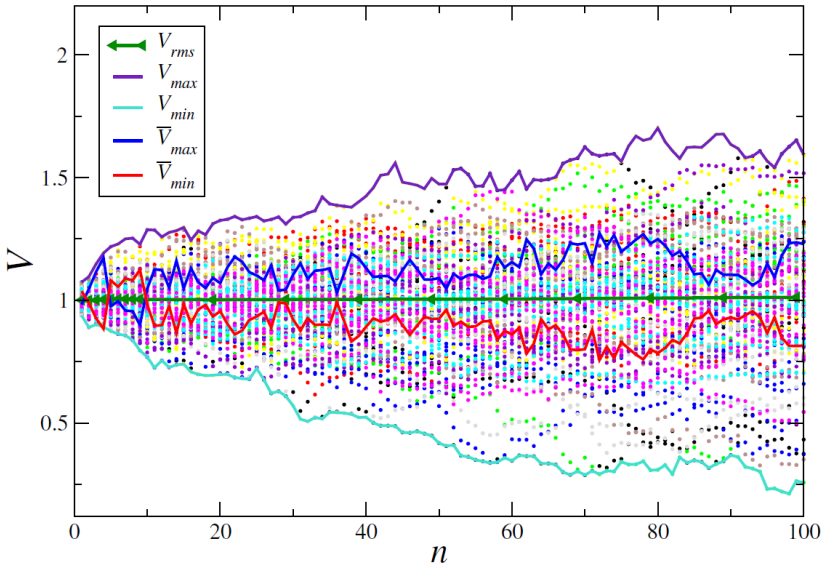

Fig. 4. (Color online) V_{rms}, V_{max}, V_{min}, $\overline{V}_{max}$, and $\overline{V}_{min}$ vs. n for $V_0 = 1$, $\epsilon = 0.08$, $\eta = 0.5$ and $\gamma = 1$. The circles represent different trajectories traversed by 10 initial conditions for each color.

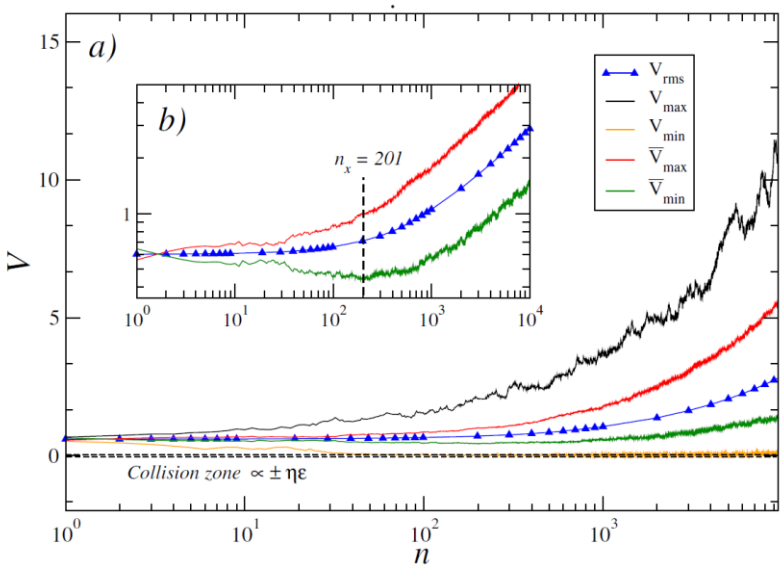

Fig. 5. (Color online) Evolution of the velocities and their averages during the dynamics of the system for the conservative case. a) V_{rms}, V_{max}, V_{min}, $\overline{V}_{max}$, and $\overline{V}_{min}$ vs. n for $V_0 = 0.6$, $\epsilon = 0.08$, $\eta = 0.5$ and $\gamma = 1$. Panel b) shows a magnified view of the crossover iteration n_x obtained from the green curve.

This limit is given by the velocity of the moving boundary itself, given by Eq. (7), that is, the particles cannot have velocities lower than that of the boundary after the collision since, upon colliding, their velocities would be increased by the boundary itself. Thus, once the particles reach the lower limit, their value can only increase, leading to the observed symmetry breaking, where the distribution ceases to be Gaussian, as shown in blue in Fig. 6. This behavior is also observed in Fig. 5 for the curves V_{max} and V_{min}, with the first growing unboundedly and the second oscillating around the lower limit in the collision zone $V_b \propto \pm\eta\epsilon$. Together, these behaviors lead to the power-law growth of the V_{rms} curve, in blue. The presence of a lower limit combined with the absence of an upper limit for such a system also leads, for a sufficiently large number of collisions, to the phenomenon known as superdiffusion. This phenomenon is defined by a change in the diffusion exponent β, from the normal diffusion value of 0.5 to 1, a value characteristic of ballistic transport or strongly time-correlated dynamics, as characterized by Hansen *et al*. [35]. The crossover iteration, n_x, then marks the point at which the average of the velocities reaches the lower limit. The blue distribution, for n = 100, as shown in Fig. 6, corroborates this analysis, with the appearance of a "tail" to the right of V_0. The same behavior is also corroborated by the probability density function $P(V,n)$ for the same system, shown in green in Fig. 7. This distribution has as boundary conditions $P(V,n)|_{V\to 0} = P(V,n)|_{V\to\infty} = 0$ and $P(V,n)_{n=0} = \delta(V - V_0)$, ensuring that all particles start with the same initial velocity, distributed across M different initial conditions, uniformly distributed over α, θ, and t. For a sufficiently small number of collisions, all velocities are centered around the initial velocity, according to the delta function. As the number of collisions increases, this distribution gradually "flattens" remaining symmetric for n = 100.

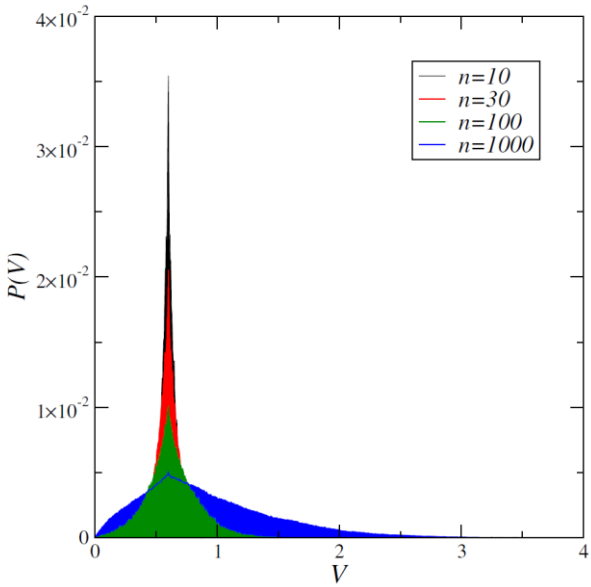

Fig. 6. (Color online) Probability density for a set of 3500 particles after n = 10, 30, 100 and 1000 collisions. The parameters used were V_0 = 0.6, ϵ = 0.08, η = 0.5, p = 3 and γ = 1.

4. Dissipative Case

We now extend the previous analysis to the dissipative case, i.e., γ < 1, seeking to identify how dissipation affects the velocity dynamics and symmetry properties of the system.

As observed in the V_{rms} curves in Section 2, the velocities now reach a plateau for a sufficiently large number of collisions. A sufficiently low initial velocity, V_0 = 0.2, was chosen to exhibit both transitions: from the initial plateau at V_0 to the growth regime at n_1 and from the growth regime to the saturation regime at n_2.

Fig. 7 presents the behaviors of V_{rms}, V_{max}, V_{min}, $\overline{V}_{max}$ and $\overline{V}_{min}$ for p = 3, ϵ = 0.1, η = 0.2, and γ = 0.999, ensuring that we are on the verge of the transition between the conservative and dissipative dynamics.

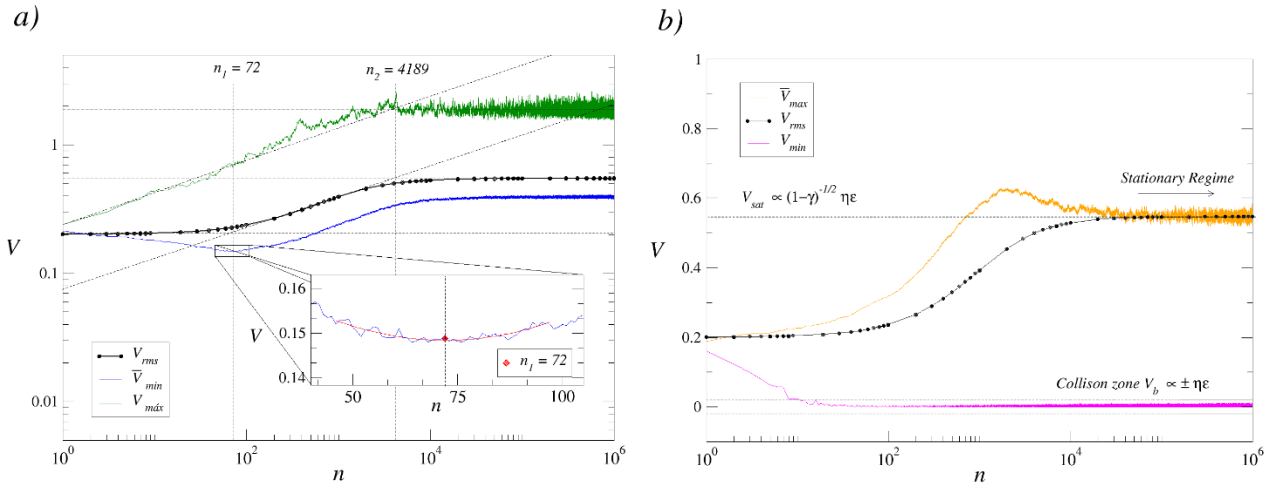

Fig. 7. (Color online) Evolution of the velocities and their averages during the dynamics of the system for the dissipative case. a) V_{rms}, V_{max}, and $\overline{V}_{min}$ vs. n for V_0 = 0.2, ϵ = 0.1, η = 0.2, and γ = 0.999, with a magnified view of the crossover iteration n_1 obtained from the quadratic fit (in red) of the blue curve. As shown, the crossover iterations n_1 and n_2 were also obtained from the black and green curves. b) V_{rms}, $\overline{V}_{max}$ and V_{min} for the same parameters, with V_{sat} and the collision zone at V_b indicated by dotted lines.

Fig. 7a) shows the crossover iterations n_1 and n_2 obtained by two different methods: (i) from the intersection between the growth and saturation regimes of the curves V_{max} and V_{rms}, represented by the dotted lines (ii) from the minimum of the $\overline{V}_{min}$ through a quadratic fit, shown in red. The results found show complete compatibility.

As for Fig. 7b), the curves of V_{rms}, $\overline{V}_{max}$ and V_{min} are shown, where the latter presents the same behavior observed in Fig. 5, a decay until the lower limit region, given by the boundary velocity. From this point on, V_{min} oscillates within the collision region described by $V_b \propto \pm\eta\epsilon$. The velocity $\overline{V}_{max}$ presents a growth pattern until the moment in which it crosses the line given by the saturation velocity. This region marks, physically, velocities large enough that the losses due to dissipation, even if minimal, are comparable to the velocities themselves. The saturation velocity V_{sat} is then reached, after a sufficiently large number of collisions, not only for V_{rms} but also for $\overline{V}_{max}$. Such $V_{sat} \propto (1-\gamma)^{-1/2}\eta\epsilon$ acts as an upper limit for the system's velocity. This behavior is corroborated by the distributions presented in Fig. 8, constructed for V_0 = 0.6, ϵ = 0.08, η = 0.5, and p = 3. The figures are robust to the increase in collisions up to n = 50, 000 and to the variation of γ near the transition. For a sufficiently small number of collisions, the behavior observed in Fig. 6 is recovered; the distribution is centered symmetrically around the initial velocity V_0. The increase in collisions leads to the asymmetric behavior observed in items a)–c), an upper limit inhibits the curve from spreading indefinitely, reaching a steady state, as indicated in Fig. 7b). The behavior is also consistent with the variation of the restitution coefficient γ, which controls how fast such a distribution flattens. Fig. 8b) shows, for the same n = 5, 000, a distribution that progressively spreads out as γ increases, approaching the transition at γ = 1. It is essential to mention that this upper limit given by the saturation velocity V_{sat} is also proportional to γ, allowing curves d)–f) to reach different maximum values.

The same distribution can also be characterized analytically by Fonseca *et al.* [36]

$$P(V,n) = \frac{\tau}{\sqrt{4\pi D_n}}[e^{(\frac{-(V-V_0)^2}{4D_n})} - e^{(\frac{-(V+V_0)^2}{4D_n})}], \quad (10)$$

where τ = erf$(\frac{V_0}{\sqrt{4D_n}})$ is a normalization constant. This distribution retrieves the behavior $P(V,0) = \delta(V - V_0)$ and is constructed using the images method, assuming that there is a "barrier" at $+\infty$ and an absorbing or reflecting one at 0. This equation only works as expected when the system is sufficiently close to the transition, i.e. $\gamma \to 1$ since its obtaining arises from the solution of the diffusion equation $\frac{\partial P(V,n)}{\partial_n} = D\frac{\partial^2 P(V,n)}{\partial V^2}$. In the conservative case, we would have to resort to a construction where such an upper limit does not exist, with only one lower "barrier". It is also important to mention that the mechanisms presented so far seek to describe the behavior of the system on the verge of transition. Therefore, such results are not adequate to describe the system for values of γ far from 1. In strictly conservative or dissipative regimes, the modeling presented in Section 2 is sufficient.

The symmetry breaking that occurs at the transition point $\gamma = 1$ is then characterized by the change from a regime where there is only a lower limit for the velocities given by the boundary, in the conservative case, to a second regime, dissipative, where the same lower limit exists alongside an upper limit given by the saturation velocity. This behavior can be verified both in the curves V_{rms}, V_{max}, V_{min}, $\overline{V}_{max}$, $\overline{V}_{min}$ and in the distribution $P(V,n)$. A straightforward comparison between Figs. 5 and 7 show the same behavior for V_{min} and $\overline{V}_{min}$, representing the lower limit, and significantly different behaviors for V_{max} and $\overline{V}_{max}$. After an initial growth, the latter reaches a steady state for a sufficiently large number of collisions due to the dissipation effect, suppressing the FA. Other billiards framed by the LRA conjecture, such as the elliptical and annular [17, 37], that exhibit FA for the conservative case, which can then be suppressed by dissipation, may also be framed by this characterization.

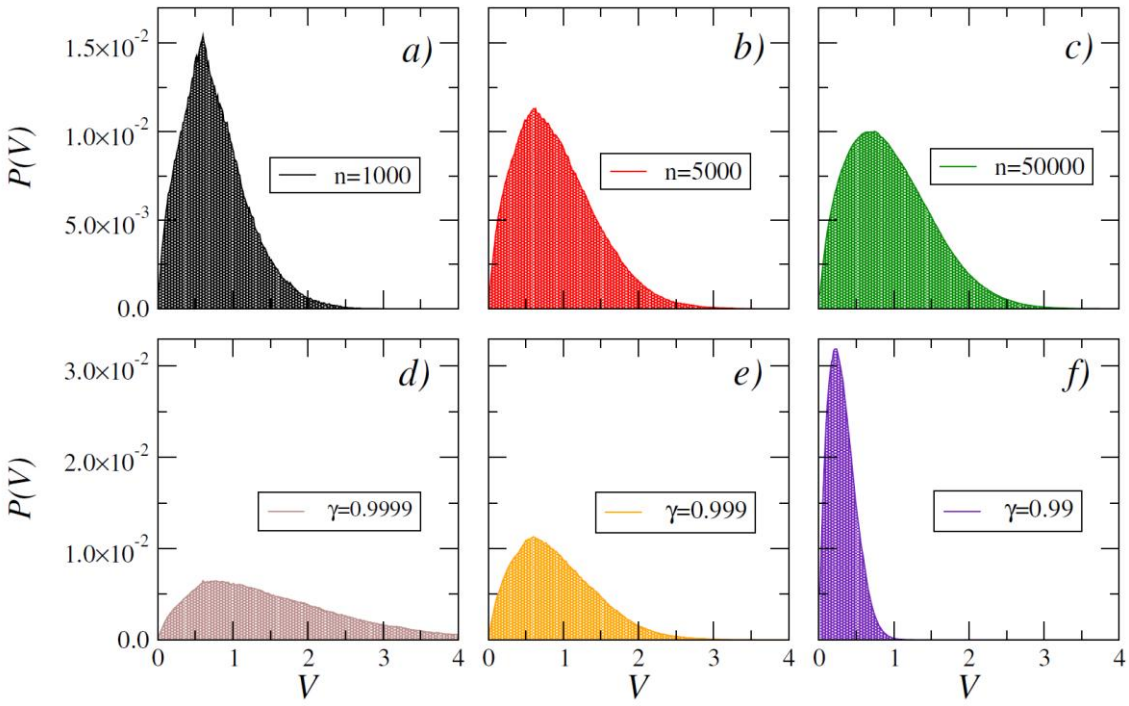

Fig. 8. (Color online) Probability density for a set of 3500 particles for $V_0 = 0.6$, $\epsilon = 0.08$, $\eta = 0.5$, $p = 3$. a), b), and c) show the behavior for $\gamma = 0.999$ and $n = 1000$, $n = 5000$, and $n = 50{,}000$ collisions. Figs. d), e) and f), for $n = 5000$ collisions, show the behavior for $\gamma = 0.99$, $\gamma = 0.999$ and $\gamma = 0.9999$.

5. Summary and Conclusions

We characterized the symmetry breaking from a dissipative to a non-dissipative dynamics for a time-dependent billiard. The transition leads to an upper limit alongside the preexisting lower limit defined by the velocity of the boundary. The discussion enabled us to identify the role of the velocity distribution in such symmetry breaking, with the quantity V min marking the crossover iteration as the point where it stops decreasing and starts increasing alongside the V_{max}. This behavior leads to the power law growth regime for V_{rms} and is exhibited in the conservative and dissipative scenarios. The quantities V_{max} and V_{max}, on the other hand, exhibit significant change after the transition, reaching an upper limit and eventual saturation for the dissipative case, suppressing the FA. The distributions $P(V)$, phenomenological and analytical, corroborate this analysis. Characterizing the symmetry-breaking mechanisms allows a better understanding of the continuous phase transitions exhibited for these systems, marked by scaling invariance, with scaling laws and critical exponents defining the criticality near the transition. These results may be relevant for systems where time-dependent boundary interactions play a key role and may induce similar symmetry-breaking mechanisms and phase transitions, such as optical billiards, microwave cavities, and plasma confinement devices, as well as other billiards framed by the LRA conjecture.

Conflict of Interest

The authors declare no conflict of interest.

Author Contributions

The authors jointly formulated the research problem. AKPF proposed the approach to address the problem, and EDL contributed to the development of the methodological framework and validation strategy. Numerical simulations and figure preparation were primarily carried out by AKPF, with adjustments and refinements made in collaboration with EDL. The manuscript was written by AKPF and revised with contributions and feedback from EDL. Both authors reviewed and approved the final version of the manuscript.

Funding

A.K.P.F. acknowledges CAPES for financial support under Grant No. 88887.990665/2024–00. E.D.L. acknowledges support from Brazilian agencies CNPq (No. 301318/2019–0, 304398/2023–3) and FAPESP (No. 2019/14038–6 and No. 2021/09519–5).

References

[1] Fröhlich, J. (2024). Phase transitions, spontaneous symmetry breaking, and Goldstone's theorem. In T. Chakraborty (Ed.), *Encyclopedia of Condensed Matter Physics* (2nd ed., pp. 158–173). Academic Press.

[2] Chaikin, P. M., & Lubensky, T. C. (1995). *Principles of Condensed Matter Physics*. Cambridge University Press.

[3] Larsen, P. G., & Nielsen, A. E. B. (2024). Phase transitions in quantum many-body scars. *Physical Review Research*, *6(4)*, L042007. https://doi.org/10.1103/PhysRevResearch.6.L042007

[4] Adachi, K., Takasan, K., & Kawaguchi, K. (2022). Activity-induced phase transition in a quantum many-body system. *Physical Review Research*, *4(1)*, 013194. https://doi.org/10.1103/PhysRevResearch.4.013194

[5] Sadhasivam, V. G., Suzuki, F., Yan, B., & Sinitsyn, N. A. (2024). Parametric tuning of quantum phase transitions in ultracold reactions. *Nature Communications*, 15, 10246. https://doi.org/10.1038/s41467-024-54701-w

[6] Aarts, G., Aichelin, J., Allton, C., Athenodorou, A., Bachtis, D., Bonanno, C., Brambilla, N., Bratkovskaya, E.,

Bruno, M., Caselle, M., Conti, C., Contino, R., Cosmai, L., Cuteri, F., Del Debbio, L., D'Elia, M., Dimopoulos, P., Di Renzo, F., Galatyuk, T., Wiese, U.-J., *et al.* (2023). Phase transitions in particle physics: Results and perspectives from lattice quantum chromo-dynamics. *Progress in Particle and Nuclear Physics*, *133*, 104070. https://doi.org/10.1016/j.ppnp.2023.104070

[7] Raz, T., & Levine, R. D. (2023). The essence of phase transitions in condensed matter by an information theoretic approach. *Proceedings of the National Academy of Sciences*, *120(50)*, e2310281120. https://doi.org/10.1073/pnas.2310281120

[8] Reeves, G., & Pfister, H. D. (2021). Understanding phase transitions via mutual information and MMSE. In M. R. D. Rodrigues & Y. C. Eldar (Eds.). *Information-Theoretic Methods in Data Science* (pp. 197–228). Cambridge University Press.

[9] Leonel, E. D., Penalva, J., Teixeira, R. M., Costa Filho, R. N., Silva, M. R., & De Oliveira, J. A. (2015). A dynamical phase transition for a family of Hamiltonian mappings: A phenomenological investigation to obtain the critical exponents. *Physics Letters A*, *379(28–29)*, 1808–1812. https://doi.org/10.1016/j.physleta.2015.05.004

[10] Oliveira, D. F., & Leonel, E. D. (2013). Some dynamical properties of a classical dissipative bouncing ball model with two nonlinearities. *Physica A: Statistical Mechanics and its Applications*, *392(8)*, 1762–1769. https://doi.org/10.1016/j.physa.2012.12.002

[11] Sethna, J. P. (2021). *Statistical Mechanics: Entropy, Order Parameters, and Complexity* (2nd ed.). Oxford University Press.

[12] Landau, L. D. (1969). *Statistical Physics* (Vol. 6). Pergamon Press.

[13] Ehrenfest, P. (1933). Phase transitions in the usual and generalized sense, classified according to the singularities of the thermodynamic potential. *Proceedings of the Amsterdam Academy*, *36*, 153–157.

[14] Reif, F. (2009). *Fundamentals of Statistical and Thermal Physics*. Waveland Press.

[15] Leonel, E. D., Yoshida, M., & de Oliveira, J. A. (2020). Characterization of a continuous phase transition in a chaotic system. *EPL (Europhysics Letters)*, *131(2)*, 20002. https://doi.org/10.1209/0295-5075/131/20002

[16] Miranda, L. K., Kuwana, C. M., Huggler, Y. H., Fonseca, A. K., Yoshida, M., Oliveira, J. A., & Leonel, E. D. (2022). A short review of phase transition in a chaotic system. *The European Physical Journal Special Topics*, *231(2)*, 167–177. https://doi.org/10.1140/epjs/s11734-021-00390-9

[17] Dembowski, C., Gräf, H.-D., Heine, A., Hofferbert, R., Rehfeld, H., & Richter, A. (2000). First experimental evidence for chaos-assisted tunneling in a microwave annular billiard. *Physical Review Letters*, *84(5)*, 867–870. https://doi.org/10.1103/PhysRevLett.84.867

[18] Berglund, N., & Kunz, H. (1996). Integrability and ergodicity of classical billiards in a magnetic field. *Journal of Statistical Physics*, *83(1–2)*, 81–126. https://doi.org/10.1007/BF02199143

[19] Chernov, N., & Markarian, R. (2006). *Chaotic Billiards*. American Mathematical Society.

[20] Berry, M. V. (1981). Regularity and chaos in classical mechanics, illustrated by three deformations of a circular 'billiard'. *European Journal of Physics*, *2(2)*, 91–102. https://doi.org/10.1088/0143-0807/2/2/005

[21] Bunimovich, L., & Dettmann, C. (2005). Open circular billiards and the Riemann hypothesis. *Physical Review Letters*, *94(10)*, 100201. https://doi.org/10.1103/PhysRevLett.94.100201

[22] Dettmann, C. P., & Georgiou, O. (2009). Survival probability for the stadium billiard. *Physica D: Nonlinear Phenomena*, *238(23–24)*, 2395–2403. https://doi.org/10.1016/j.physd.2009.09.008

[23] Lozej, Č., & Robnik, M. (2018). Aspects of diffusion in the stadium billiard. *Physical Review E*, *97(1)*, 012206. https://doi.org/10.1103/PhysRevE.97.012206

[24] Lopac, V., Mrkonjić, I., & Radić, D. (2002). Chaotic dynamics and orbit stability in the parabolic oval

billiard. *Physical Review E*, *66(3)*, 036202. https://doi.org/10.1103/PhysRevE.66.036202

[25] Lichtenberg, A. J., & Lieberman, M. A. (2013). *Regular and Chaotic Dynamics* (2nd ed.). Springer Science & Business Media.

[26] Wang, S., Liu, S., Liu, Y., Xiao, S., Wang, Z., Fan, Y., Han, J., Ge, L., & Song, Q. (2021). Direct observation of chaotic resonances in optical microcavities. *Light: Science & Applications*, *10(1)*, 135. https://doi.org/10.1038/s41377-021-00573-y

[27] Chandramouli, R. S., Srivastav, R. K., & Kumar, S. (2020). Electronic transport in chaotic mesoscopic cavities: A kwant and random matrix theory based exploration. *Chaos: An Interdisciplinary Journal of Nonlinear Science*, *30(12)*, 123120. https://doi.org/10.1063/5.0026039

[28] Exner, P., Hejčák, P., & Šeba, P. (2006). Approximations by graphs and emergence of global structures. *Reports on Mathematical Physics*, *57(3)*, 445–456. https://doi.org/10.1016/S0034-4877(06)80040-5

[29] Miao, F., Wijeratne, S., Zhang, Y., Coskun, U. C., Bao, W., & Lau, C. N. (2007). Phase-coherent transport in graphene quantum billiards. *Science*, *317(5844)*, 1530–1533. https://doi.org/10.1126/science.1144359

[30] Loskutov, A. Y., Ryabov, A. B., & Akinshin, L. G. (1999). Mechanism of Fermi acceleration in dispersing billiards with time-dependent boundaries. *Journal of Experimental and Theoretical Physics*, *89(6)*, 966–974. https://doi.org/10.1134/1.558980

[31] Loskutov, A., Ryabov, A., & Akinshin, L. (2000). Properties of some chaotic billiards with time-dependent boundaries. *Journal of Physics A: Mathematical and General*, *33(44)*, 7973–7990. https://doi.org/10.1088/0305-4470/33/44/305

[32] Oliveira, D. F., & Leonel, E. D. (2010). Suppressing Fermi acceleration in a two-dimensional non-integrable time-dependent oval-shaped billiard with inelastic collisions. *Physica A: Statistical Mechanics and its Applications*, *389(*5), 1009–1015. https://doi.org/10.1016/j.physa.2009.11.017

[33] Leonel, E. D., Galia, M. V. C., Barreiro, L. A., & Oliveira, D. F. (2016). Thermodynamics of a time-dependent and dissipative oval billiard: A heat transfer and billiard approach. *Physical Review E*, *94(6)*, 062211. https://doi.org/10.1103/PhysRevE.94.062211

[34] Leonel, E. D. (2022). *Scaling laws in dynamical systems*. Higher Education Press.

[35] Hansen, M., Ciro, D., Caldas, I. L., & Leonel, E. D. (2018). Explaining a changeover from normal to super diffusion in time-dependent billiards. *Europhysics Letters*, *121(4)*, 40003. https://doi.org/10.1209/0295-5075/121/40003

[36] Fonseca, A. K. P., Silveira, F. A. O., Kuwana, C. M., Oliveira, D. F. M., & Leonel, E. D. (2025). Transition from bounded to unbounded energy in a time-dependent billiard. *Physical Review E*, *101(1)*, 012201. https://doi.org/10.1103/PhysRevE.101.012201

[37] Oliveira, D. F., & Robnik, M. (2012). Scaling invariance in a time-dependent elliptical billiard. *International Journal of Bifurcation and Chaos*, *22(11)*, 1250207. https://doi.org/10.1142/S0218127412502076